LETTER

doi:10.1038/nature19802

Two distinct RNase activities of CRISPR–C2c2 enable guide–RNA processing and RNA detection

Alexandra East-Seletsky[1]*, Mitchell R. O'Connell[1]*, Spencer C. Knight[2], David Burstein[3], Jamie H. D. Cate[1,2,4], Robert Tjian[1,5,6,7] & Jennifer A. Doudna[1,2,4,6,8]

Bacterial adaptive immune systems use CRISPRs (clustered regularly interspaced short palindromic repeats) and CRISPR-associated (Cas) proteins for RNA-guided nucleic acid cleavage[1,2]. Although most prokaryotic adaptive immune systems generally target DNA substrates[3–5], type III and VI CRISPR systems direct interference complexes against single-stranded RNA substrates[6–9]. In type VI systems, the single-subunit C2c2 protein functions as an RNA-guided RNA endonuclease (RNase)[9,10]. How this enzyme acquires mature CRISPR RNAs (crRNAs) that are essential for immune surveillance and how it carries out crRNA-mediated RNA cleavage remain unclear. Here we show that bacterial C2c2 possesses a unique RNase activity responsible for CRISPR RNA maturation that is distinct from its RNA-activated single-stranded RNA degradation activity. These dual RNase functions are chemically and mechanistically different from each other and from the crRNA-processing behaviour of the evolutionarily unrelated CRISPR enzyme Cpf1 (ref. 11). The two RNase activities of C2c2 enable multiplexed processing and loading of guide RNAs that in turn allow sensitive detection of cellular transcripts.

The first step of CRISPR immune surveillance requires the processing of precursor crRNA transcripts (pre-crRNAs), consisting of repeat sequences flanking viral spacer sequences, into individual mature crRNAs that each contain a single spacer[12–14]. CRISPR systems use three known mechanisms to produce mature crRNAs: a dedicated endonuclease (for example, Cas6 or Cas5d in type I and III systems)[15–17], coupling of a host endonuclease (for example, RNase III with a trans-activating crRNA in type II systems)[18], or RNase activity intrinsic to the effector enzyme itself (for example, Cpf1 in type V systems)[11].

Because type VI CRISPR loci lack an obvious Cas6- or Cas5d-like endonuclease or trans-activating crRNA[10], we wondered whether C2c2 itself might possess pre-crRNA processing activity, and if so, whether the mechanism would be distinct from Cpf1, an unrelated class 2 CRISPR effector that can process pre-crRNAs[11]. Using purified recombinant C2c2 protein homologues from three distinct branches of the C2c2 protein family (Fig. 1a, b, Extended Data Figs 1, 2), we found that all three enzymes cleave 5′-end radiolabelled pre-crRNA substrates consisting of a full-length consensus repeat sequence and a 20-nucleotide spacer sequence (Fig. 1c). Mapping the cleavage site for each pre-crRNA–C2c2 homologue pair revealed that processing occurs either two or five nucleotides upstream of the predicted repeat-sequence hairpin structure, depending on the C2c2 homologue (Fig. 1c, Extended Data Fig. 3a). Notably, these mapped 5′-cleavage sites do not agree with the

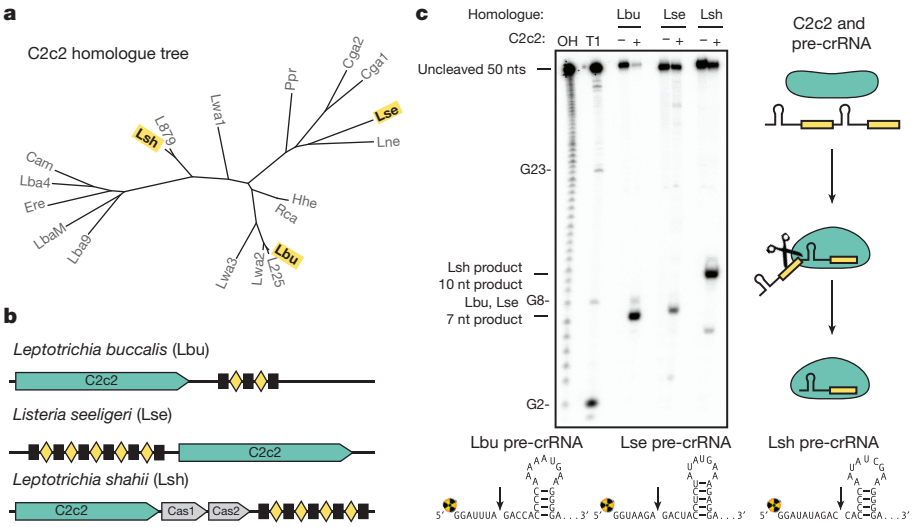


Figure 1 | C2c2 proteins process precursor crRNA transcripts to generate mature crRNAs. a, Maximum-likelihood phylogenetic tree of C2c2 proteins. Homologues used in this study are highlighted in yellow. **b**, Diagram of the type VI CRISPR loci used in this study. Black rectangles denote repeat elements, yellow diamonds denote spacer sequences. Cas1 and Cas2 are only found in the genomic vicinity of LshC2c2. **c**, C2c2-mediated cleavage of pre-crRNA derived from the LbuC2c2, LseC2c2 and LshC2c2 CRISPR repeat loci. OH, alkaline hydrolysis ladder; T1, RNase T1 hydrolysis ladder. Processing cleavage reactions were performed with 100 nM C2c2 and <1 nM pre-crRNA. Schematic of cleavage is depicted on the right and predicted pre-crRNA secondary structures are shown below, with arrows indicating the mapped C2c2 cleavage sites (nt, nucleotides).

[1]Department of Molecular and Cell Biology, University of California, Berkeley, California 94720, USA. [2]Department of Chemistry, University of California, Berkeley, California 94720, USA. [3]Department of Earth And Planetary Sciences, University of California, Berkeley, California 94720, USA. [4]MBIB Division, Lawrence Berkeley National Laboratory, Berkeley, California 94720, USA. [5]Janelia Research Campus, Howard Hughes Medical Institute, Ashburn, Virginia 20147, USA. [6]Howard Hughes Medical Institute, University of California, Berkeley, California 94720, USA. [7]Li Ka Shing Biomedical and Health Sciences Center, University of California, Berkeley, California 94720, USA. [8]Innovative Genomics Initiative, University of California, Berkeley, California 94720, USA.
*These authors contributed equally to this work.

© 2016 Macmillan Publishers Limited, part of Springer Nature. All rights reserved.

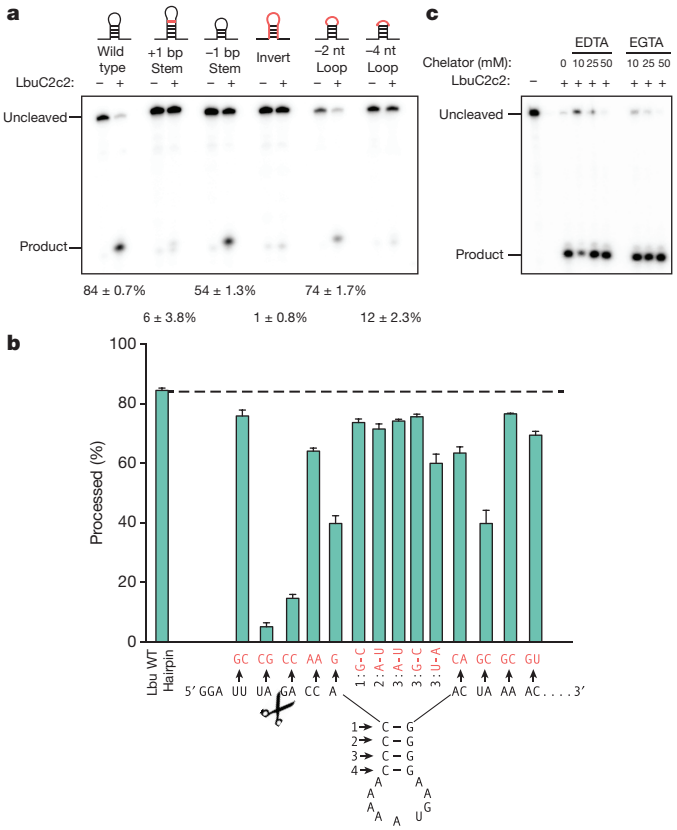


Figure 2 | LbuC2c2-mediated crRNA biogenesis depends on both structure and sequence of CRISPR repeats. a, Representative cleavage assay by LbuC2c2 on pre-crRNAs containing structural mutations within the stem and loop regions of hairpin. Processed percentages listed below are quantified at 1 h (mean ± s.d., $n = 3$). **b**, Bar graph showing the dependence of pre-crRNA processing on the CRISPR repeat sequence. The wild-type (WT) repeat sequence is shown below with individual bars representing tandem nucleotide mutations as noted in red. The cleavage site is indicated by cartoon scissors. Percentage processed was measured after 1 h (mean ± s.d., $n = 3$). **c**, Divalent metal ion dependence of the crRNA processing reaction was tested by the addition of 10–50 mM EDTA and EGTA to standard reaction conditions.

previously reported sites for *Leptotrichia shahii* (LshC2c2) or *Listeria seeligeri* (LseC2c2) pre-crRNAs[10]. Our analysis of the RNA sequencing dataset in ref. 10 indicates agreement of the *in vivo* cleavage site with the *in vitro* site reported here (Extended Data Fig. 3b–i). Furthermore, cleavage assays using C2c2 from *Leptotrichia buccalis* (LbuC2c2) and a larger pre-crRNA comprising a tandem hairpin-repeat array yielded two products resulting from two separate cleavage events (Extended Data Fig. 4a), consistent with a role for C2c2 in processing precursor crRNA transcripts generated from type VI CRISPR loci.

To understand the substrate requirements and mechanism of C2c2 guide-RNA processing, we generated pre-crRNAs containing mutations in either the stem–loop or the single-stranded flanking regions of the consensus repeat sequence, and tested their ability to be processed by LbuC2c2 (Fig. 2). C2c2-catalysed cleavage was attenuated upon altering the length of the stem in the repeat region (Fig. 2a). Inversion of the stem–loop or reduction of the loop length also reduced the processing activity of C2c2, while contiguous 4-nucleotide mutations including or near the scissile bond completely abolished it (Extended Data Fig. 4b). More extensive mutational analysis of the full crRNA repeat sequence revealed two distinct regions on either side of the hairpin with marked sensitivity to base changes (Fig. 2b). By contrast, there was no dependence on the spacer sequence for kinetics of processing (Extended Data Fig. 4c). This sensitivity to both flanking regions of the hairpin is reminiscent of the sequence and structural motifs required by many Cas6 and Cas5d enzymes[12,13,19]. Cpf1, however, does not have any dependence on the 3′ hairpin flanking region, as the variable spacer region abuts the hairpin stem[11].

The processing activity of LbuC2c2 was unaffected by the presence of divalent metal ion chelators (Fig. 2c), indicative of a metal-ion-independent RNA hydrolytic mechanism. Metal-ion-independent RNA hydrolysis is typified by the formation of a 2′,3′-cyclic phosphate and a 5′-hydroxide on the 5′ and 3′ halves of the crRNA cleavage products, respectively[20]. To determine the end-group chemical identity of C2c2-processed substrates, we incubated the 5′ flanking products with T4 polynucleotide kinase, which removes 2′,3′-cyclic phosphates to leave a 3′-hydroxyl; this resulted in altered denaturing-gel migration of the 5′ flanking product, consistent with the removal of a 3′ phosphate group (Extended Data Fig. 4d). The divalent metal ion independence of the C2c2 pre-crRNA processing activity is in stark contrast with the divalent metal ion dependency of Cpf1, the only other single-protein CRISPR effector shown to perform guide processing[11]. Collectively, these data indicate that C2c2-catalysed pre-crRNA cleavage is a divalent metal-ion-independent process that probably uses a general acid–base catalysis mechanism[20].

After maturation, crRNAs typically bind with high affinity to Cas effector protein(s) to create RNA-guided surveillance complexes capable of sequence-specific nucleic acid recognition[1,2,21]. In agreement with previous work on LshC2c2 (ref. 9), LbuC2c2 catalysed efficient target RNA cleavage only when such substrates could base pair with a complementary sequence in the crRNA (Extended Data Figs 5–7). Given the promiscuous pattern of cleavage observed for C2c2 (Extended Data Fig. 6), we tested the ability of LbuC2c2 to act as a crRNA-activated non-specific RNA endonuclease in *trans* (Extended Data Fig. 5b). In marked contrast to non-target cleavage experiments performed in *cis* and consistent with observations for LshC2c2 (ref. 9), we observed rapid degradation of non-target RNA (Extended Data Fig. 5b); thus, target recognition activates C2c2 for general non-specific degradation of RNA. Importantly, the similar cleavage rates and near-identical cleavage products observed for both *cis* on-target cleavage and *trans* non-target cleavage of the same RNA substrate implicate the same nuclease centre in both activities (Extended Data Fig. 5b).

crRNA-mediated cleavage of target single-stranded RNA (ssRNA) occurs ~80-fold faster than pre-crRNA processing (Fig. 3a). In contrast to pre-crRNA processing, RNA-guided target cleavage is abolished in the presence of EDTA, indicating that this activity is divalent metal ion-dependent (Fig. 3a, Extended Data Figs 5c, 7). Given these clear differences, we reasoned that C2c2 might possess two orthogonal RNA cleavage activities: crRNA maturation, and crRNA-directed, non-specific RNA degradation. To test this hypothesis, we generated mutants within several residues within the conserved HEPN (higher eukaryotes and prokaryotes nucleotide-binding domain) motifs of LbuC2c2 (refs 9, 22–24) and assessed their pre-crRNA processing and RNA-guided RNase activities (Fig. 3, Extended Data Fig. 7d). Double and quadruple mutants (R472A, H477A, R1048A and H1053A) retained robust pre-crRNA cleavage activity (Fig. 3c), but all HEPN mutations abolished RNA-guided cleavage activity without affecting crRNA or ssRNA binding ability[9] (Extended Data Figs 7d, 8).

We sought mutations that would abrogate pre-crRNA processing activity without disrupting target RNA cleavage. Given that we were unable to predict any other potential RNase motifs beyond the HEPN motifs, and that C2c2 proteins lack homology to Cpf1, we opted to mutate charged residues throughout LbuC2c2 systematically. We identified an arginine residue (R1079A) that upon mutation resulted in severely attenuated pre-crRNA processing activity (Fig. 3c). This C2c2 mutant enzyme retained crRNA-binding ability as well as RNA target cleavage activity (Extended Data Fig. 8d, Fig. 3d). These results show that distinct active sites within the C2c2 protein catalyse pre-crRNA processing and RNA-directed RNA cleavage.

© 2016 Macmillan Publishers Limited, part of Springer Nature. All rights reserved.

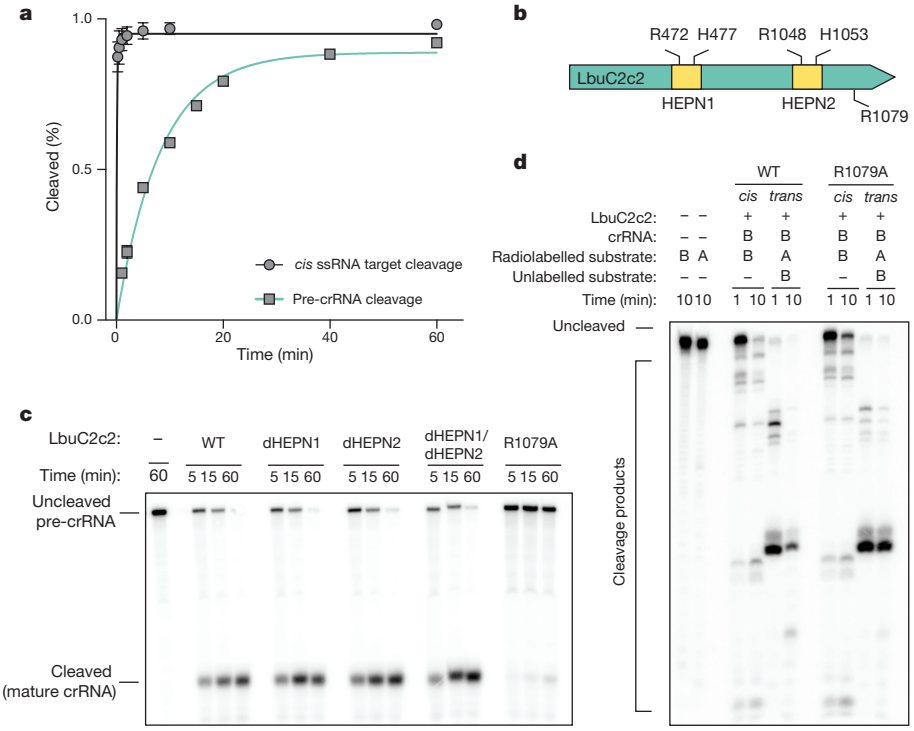


Figure 3 | LbuC2c2 contains two distinct RNase activities. a, Quantified time-course data of *cis* ssRNA target (black) and pre-crRNA (teal) cleavage by LbuC2c2. Exponential fits are shown as solid lines ($n = 3$), and the calculated pseudo-first-order rate constants (k_{obs}) (mean ± s.d.) are $9.74 \pm 1.15\ min^{-1}$ and $0.12 \pm 0.02\ min^{-1}$ for *cis* ssRNA target and pre-crRNA cleavage, respectively. **b**, LbuC2c2 architecture depicting the location of HEPN motifs and processing-deficient point mutant **c**, **d**, Representative ribonuclease activity of LbuC2c2 mutants for pre-crRNA processing in **c** and ssRNA targeting in **d** and Extended Data Fig. 6d.

We recognized that the robust RNA-stimulated cleavage of substrates by C2c2 in *trans* might be used to detect specific RNAs within a pool of transcripts. While many polymerase-based methods have been developed for RNA amplification and subsequent detection, few approaches are able to detect target RNA directly without considerable engineering or stringent design constraints for each new RNA target[20,25–27]. As a readily programmable alternative, we tested whether the RNA-guided *trans*-endonuclease activity of C2c2 could be harnessed to cleave a fluorophore quencher-labelled reporter RNA, thereby resulting in increased fluorescence upon target-RNA-triggered RNase activation (Fig. 4a). LbuC2c2 was loaded with bacteriophage λ-targeting crRNAs and tested for its ability to detect the corresponding λ ssRNA targets spiked into HeLa cell total RNA. Upon addition of as little as 1–10 pM complementary λ target RNA, a substantial crRNA-specific fluorescence increase occurred within 30 min (Fig. 4b, Extended Data Fig. 9a). Control experiments with the C2c2–crRNA complex either alone or in the presence of crRNA and a non-complementary target RNA resulted in negligible increases in fluorescence relative to a positive control (Fig. 4b, Extended Data Fig. 9a). At 10 pM concentration of a λ target RNA, only ~0.02% of the C2c2–crRNA complex is predicted to be in the active state, yet the observed fluorescent signal reflected ~25–50% cleavage of the reporter RNA substrate, depending on the RNA target. Fragment size resolution of the background RNA in these reactions revealed considerable degradation, even on highly structured tRNAs (Extended Data Fig. 9b). Since reporter RNA cleavage occurs in the presence of a vast excess of unlabelled RNA, we conclude that LbuC2c2 is a robust multiple-turnover enzyme capable of at least 10^4 turnovers per target RNA recognized. Thus, in contrast to previous observations[9], crRNA-directed *trans* cleavage is potent and detectable even at extremely low levels of activated protein.

To extend this LbuC2c2 RNA detection system, we designed a crRNA to target endogenous β-actin mRNA. We observed a measurable fluorescence increase in the presence of human total RNA relative to *Escherichia coli* total RNA, demonstrating the specificity of this method (Fig. 4c). Furthermore, given that C2c2 processes its own guide, we combined pre-crRNA processing and RNA detection in a single reaction by designing tandem crRNA-repeat-containing spacers complementary to target RNAs A and λ2. LbuC2c2 incubated with this unprocessed tandem guide RNA in the detection assay generated a substantial fluorescence increase similar in magnitude and sensitivity to experiments using mature crRNAs (Fig. 4b, d). Taken together, these data highlight the exciting opportunity to take advantage of the two distinct RNase activities of C2c2 for a range of biotechnological applications (Fig. 4e).

In bacteria, C2c2 probably operates as a sentinel for viral RNAs[9]. We propose that when invasive transcripts are detected within the host cell via base pairing with crRNAs, C2c2 is activated for promiscuous cleavage of RNA in *trans* (Fig. 4e). This bears notable similarity to RNase L and caspase defence mechanisms in eukaryotes, in which a cellular signal triggers promiscuous ribonucleolytic and proteolytic degradation, respectively, within the host cell, leading to apoptosis[28,29]. While the RNA targeting mechanisms of type III CRISPR systems generally result in RNA cleavage within the protospacer–guide duplex[8,30], recent examples of associated nucleases Csx1 (ref. 23) and Csm6 (ref. 24) provide compelling parallels between the type VI systems and the multi-component type III inference complexes.

Our data show that CRISPR C2c2 proteins represent a class of enzyme capable of two separate RNA recognition and cleavage activities. Efficient pre-crRNA processing requires sequence and structural motifs within the CRISPR repeat that prevent non-endogenous crRNA loading and helps to reduce the potential toxicity of this potent RNase. The entirely different pre-crRNA processing mechanisms of C2c2 and the type V CRISPR effector protein Cpf1 indicate that each protein family has converged upon independent activities encompassing both the processing and interference functions of their respective CRISPR pathways. Furthermore, the two distinct catalytic capabilities of C2c2 can be harnessed together for RNA detection, as the activation of C2c2 to cleave thousands of *trans* RNAs for every target RNA detected enables potent signal amplification. The capacity of C2c2 to process its own guide RNAs from arrays could also allow the use of tissue-specific polymerase II promoters for guide expression, in addition to target multiplexing for a wide range of applications. The C2c2 enzyme is unique within bacterial adaptive immunity for its dual RNase activities, and highlights the utility of harnessing CRISPR proteins for precise nucleic acid manipulation in cells and cell-free systems.

© 2016 Macmillan Publishers Limited, part of Springer Nature. All rights reserved.

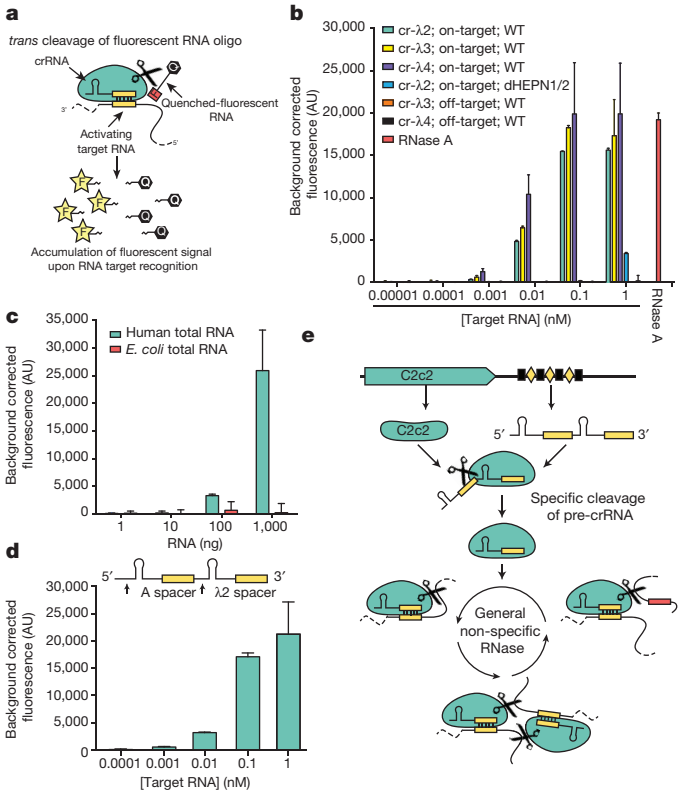


Figure 4 | C2c2 provides sensitive detection of transcripts in complex mixtures. a, Illustration of LbuC2c2 RNA detection approach using a quenched fluorescent RNA reporter. **b**, Quantification of fluorescence signal generated after 30 min by wild-type or catalytically dead (dHEPN1/2) LbuC2c2 loaded with either a λ2-, λ3- or λ4-targeting crRNA (cr-; as indicated) in the presence of varying concentrations of λ2−λ4 target ssRNA and human total RNA. RNase A shown as positive RNA degradation control (mean ± s.d., $n = 3$). AU, arbitrary units. **c**, Quantification of fluorescence signal generated by LbuC2c2 loaded with a β-actin targeting crRNA after 3 h for varying amounts of human total RNA or bacterial total RNA (as a β-actin-null negative control) (mean ± s.d., $n = 3$). **d**, Tandem pre-crRNA processing also enables RNA detection (mean ± s.d., $n = 3$). **e**, Model of the type VI CRISPR pathway highlighting both of the C2c2 RNase activities.

Online Content Methods, along with any additional Extended Data display items and Source Data, are available in the online version of the paper; references unique to these sections appear only in the online paper.

Received 14 June; accepted 24 August 2016.
Published online 26 September; corrected online 12 October 2016 (see full-text HTML version for details).

1. van der Oost, J., Westra, E. R., Jackson, R. N. & Wiedenheft, B. Unravelling the structural and mechanistic basis of CRISPR-Cas systems. *Nat. Rev. Microbiol.* **12,** 479–492 (2014).
2. Wright, A. V., Nuñez, J. K. & Doudna, J. A. Biology and applications of CRISPR systems: harnessing nature's toolbox for genome engineering. *Cell* **164,** 29–44 (2016).
3. Brouns, S. J. J. *et al.* Small CRISPR RNAs guide antiviral defense in prokaryotes. *Science* **321,** 960–964 (2008).
4. Marraffini, L. A. & Sontheimer, E. J. CRISPR interference limits horizontal gene transfer in staphylococci by targeting DNA. *Science* **322,** 1843–1845 (2008).
5. Garneau, J. E. *et al.* The CRISPR/Cas bacterial immune system cleaves bacteriophage and plasmid DNA. *Nature* **468,** 67–71 (2010).
6. Hale, C. R. *et al.* RNA-guided RNA cleavage by a CRISPR RNA-Cas protein complex. *Cell* **139,** 945–956 (2009).
7. Staals, R. H. J. *et al.* Structure and activity of the RNA-targeting type III-B CRISPR-Cas complex of *Thermus thermophilus*. *Mol. Cell* **52,** 135–145 (2013).
8. Samai, P. *et al.* Co-transcriptional DNA and RNA cleavage during type III CRISPR-Cas immunity. *Cell* **161,** 1164–1174 (2015).
9. Abudayyeh, O. O. *et al.* C2c2 is a single-component programmable RNA-guided RNA-targeting CRISPR effector. *Science* **353,** aaf5573 (2016).
10. Shmakov, S. *et al.* Discovery and functional characterization of diverse class 2 CRISPR-Cas systems. *Mol. Cell* **60,** 385–397 (2015).
11. Fonfara, I., Richter, H., Bratovič, M., Le Rhun, A. & Charpentier, E. The CRISPR-associated DNA-cleaving enzyme Cpf1 also processes precursor CRISPR RNA. *Nature* **532,** 517–521 (2016).
12. Li, H. Structural principles of CRISPR RNA processing. *Structure* **23,** 13–20 (2015).
13. Charpentier, E., Richter, H., van der Oost, J. & White, M. F. Biogenesis pathways of RNA guides in archaeal and bacterial CRISPR-Cas adaptive immunity. *FEMS Microbiol. Rev.* **39,** 428–441 (2015).
14. Hochstrasser, M. L. & Doudna, J. A. Cutting it close: CRISPR-associated endoribonuclease structure and function. *Trends Biochem. Sci.* **40,** 58–66 (2015).
15. Carte, J., Wang, R., Li, H., Terns, R. M. & Terns, M. P. Cas6 is an endoribonuclease that generates guide RNAs for invader defense in prokaryotes. *Genes Dev.* **22,** 3489–3496 (2008).
16. Haurwitz, R. E., Jinek, M., Wiedenheft, B., Zhou, K. & Doudna, J. A. Sequence- and structure-specific RNA processing by a CRISPR endonuclease. *Science* **329,** 1355–1358 (2010).
17. Nam, K. H. *et al.* Cas5d protein processes pre-crRNA and assembles into a cascade-like interference complex in subtype I-C/Dvulg CRISPR-Cas system. *Structure* **20,** 1574–1584 (2012).
18. Deltcheva, E. *et al.* CRISPR RNA maturation by trans-encoded small RNA and host factor RNase III. *Nature* **471,** 602–607 (2011).
19. Fonfara, I. *et al.* Phylogeny of Cas9 determines functional exchangeability of dual-RNA and Cas9 among orthologous type II CRISPR-Cas systems. *Nucleic Acids Res.* **42,** 2577–2590 (2014).
20. Yang, W. Nucleases: diversity of structure, function and mechanism. *Q. Rev. Biophys.* **44,** 1–93 (2011).
21. Jinek, M. *et al.* A programmable dual-RNA-guided DNA endonuclease in adaptive bacterial immunity. *Science* **337,** 816–821 (2012).
22. Anantharaman, V., Makarova, K. S., Burroughs, A. M., Koonin, E. V. & Aravind, L. Comprehensive analysis of the HEPN superfamily: identification of novel roles in intra-genomic conflicts, defense, pathogenesis and RNA processing. *Biol. Direct* **8,** 15 (2013).
23. Sheppard, N. F., Glover, C. V. C., III, Terns, R. M. & Terns, M. P. The CRISPR-associated Csx1 protein of *Pyrococcus furiosus* is an adenosine-specific endoribonuclease. *RNA* **22,** 216–224 (2016).
24. Niewoehner, O. & Jinek, M. Structural basis for the endoribonuclease activity of the type III-A CRISPR-associated protein Csm6. *RNA* **22,** 318–329 (2016).
25. Cordray, M. S. & Richards-Kortum, R. R. Emerging nucleic acid-based tests for point-of-care detection of malaria. *Am. J. Trop. Med. Hyg.* **87,** 223–230 (2012).
26. Rohrman, B. A., Leautaud, V., Molyneux, E. & Richards-Kortum, R. R. A lateral flow assay for quantitative detection of amplified HIV-1 RNA. *PLoS One* **7,** e45611 (2012).
27. Yan, L. *et al.* Isothermal amplified detection of DNA and RNA. *Mol. Biosyst.* **10,** 970–1003 (2014).
28. McIlwain, D. R., Berger, T. & Mak, T. W. Caspase functions in cell death and disease. *Cold Spring Harb. Perspect. Biol.* **5,** a008656 (2013).
29. Choi, U. Y., Kang, J.-S., Hwang, Y. S. & Kim, Y.-J. Oligoadenylate synthase-like (OASL) proteins: dual functions and associations with diseases. *Exp. Mol. Med.* **47,** e144 (2015).
30. Zhang, J., Graham, S., Tello, A., Liu, H. & White, M. F. Multiple nucleic acid cleavage modes in divergent type III CRISPR systems. *Nucleic Acids Res.* **44,** 1789–1799 (2016).

Supplementary Information is available in the online version of the paper.

Acknowledgements We thank the QB3 MacroLab for assistance with cloning of C2c2 constructs; N. Ma and K. Zhou for technical assistance; S. N. Floor, S. C. Strutt, A. V. Wright and M. L. Hochstrasser for critical reading of the manuscript; and members of the Doudna, Cate and Tjian laboratories for discussions. S.C.K. acknowledges support from the National Science Foundation Graduate Research Fellowship Program; M.R.O. is a recipient of a C. J. Martin Overseas Early Career Fellowship from the National Health and Medical Research Council of Australia. This work was supported in part by a Frontiers Science award from the Paul Allen Institute to J.A.D., the National Science Foundation (MCB-1244557 to J.A.D.), the California Institute for Regenerative Medicine (CIRM, RB4-06016 to R.T.), and the National Institutes of Health (P50-GM102706 to J.H.D.C). R.T. and J.A.D. are Investigators of the Howard Hughes Medical Institute. J.A.D. is a co-founder of Caribou Biosciences, Editas Medicine and Intellia Therapeutics and a scientific advisor to Caribou, Intellia, eFFECTOR Therapeutics, and Driver. A.E.S., M.R.O., S.C.K., J.H.D.C. and J.A.D. have filed a patent application related to this work.

Author Contributions A.E.S., M.R.O. and S.C.K. conceived the study and designed experiments with input from J.H.D.C., R.T. and J.A.D. D.B. performed bioinformatic analyses. A.E.S. and M.R.O. executed all experimental work with assistance from S.C.K. All authors discussed the data and wrote the manuscript.

Author Information Reprints and permissions information is available at www.nature.com/reprints. The authors declare competing financial interests: details are available in the online version of the paper. Readers are welcome to comment on the online version of the paper. Correspondence and requests for materials should be addressed to J.A.D. (doudna@berkeley.edu).

Reviewer Information *Nature* thanks M. White, J. Wilusz and the other anonymous reviewer(s) for their contribution to the peer review of this work.

© 2016 Macmillan Publishers Limited, part of Springer Nature. All rights reserved.

METHODS

No statistical methods were used to predetermine sample size. The experiments were not randomized, and investigators were not blinded to allocation during experiments and outcome assessment.

C2c2 phylogenic and candidate selection. C2c2 maximum-likelihood phylogenies were computed using RAxML[31] with the PROTGAMMALG evolutionary model and 100 bootstrap samplings. Sequences were aligned by MAFFT with the 'einsi' method[32].

C2c2 protein production and purification. Expression vectors for protein purification were assembled using synthenic gBlocks ordered from Integrated DNA Technologies. The codon-optimized C2c2 genomic sequence was *N*-terminally tagged with a His_6-MBP-TEV cleavage site, with expression driven by a T7 promoter. Mutant proteins were cloned via site-directed mutagenesis of wild-type C2c2 constructs. Expression vectors were transformed into Rosetta2 *E. coli* cells grown in 2×YT broth at 37 °C. *E. coli* cells were induced during log phase with 0.5 mM ITPG, and the temperature was reduced to 16 °C for overnight expression of His-MBP-C2c2. Cells were subsequently harvested, resuspended in lysis buffer (50 mM Tris-HCl pH 7.0, 500 mM NaCl, 5% glycerol, 1 mM TCEP, 0.5 mM PMSF, and EDTA-free protease inhibitor (Roche)) and lysed by sonication, and the lysates were clarified by centrifugation. Soluble His-MBP-C2c2 was isolated over metal ion affinity chromatography, and protein-containing eluate was incubated with TEV protease at 4 °C overnight while dialyzing into ion exchange buffer (50 mM Tris-HCl pH 7.0, 250 mM KCl, 5% glycerol, 1 mM TCEP) in order to cleave off the His_6-MBP tag. Cleaved protein was loaded onto a HiTrap SP column and eluted over a linear KCl (0.25–1.5 M) gradient. Cation exchange chromatography fractions were pooled and concentrated with 30 kDa cutoff concentrators (Thermo Fisher). The C2c2 protein was further purified via size-exclusion chromatography on an S200 column and stored in gel filtration buffer (20 mM Tris-HCl pH 7.0, 200 mM KCl, 5% glycerol, 1 mM TCEP) for subsequent enzymatic assays. Expression plasmids are deposited with Addgene.

Generation of RNA. All RNAs used in this study were transcribed *in vitro* except for crRNA AES461, which was ordered synthetically (Integrated DNA Technologies) (see Extended Data Table 1, Extended Data Fig. 6). *In vitro* transcription reactions were performed as previously described with the following modifications: the T7 polymerase concentration was reduced to 10 μg ml^{-1}, and the UTP concentration was reduced to 2.5 mM[33]. Transcriptions were incubated at 37 °C for 1–2 h to reduce non-template addition of nucleotides and quenched via treatment with DNase I at 37 °C for 0.5–1 h. Transcription reactions were purified by 15% denaturing polyacrylamide gel electrophoresis (PAGE), and all RNAs were resuspended in cleavage buffer (20 mM HEPES pH 6.8, 50 mM KCl, 5 mM $MgCl_2$, and 5% glycerol). For radioactive experiments, 5′ triphosphates were removed by calf intestinal phosphate (New England Biolabs) before radiolabelling and ssRNA substrates were then 5′-end labelled using T4 polynucleotide kinase (New England Biolabs) and [γ-^{32}P]ATP (Perkin Elmer) as described previously[33].

Pre-crRNA processing assays. Pre-crRNA cleavage assays were performed at 37 °C in RNA processing buffer (20 mM HEPES pH 6.8, 50 mM KCl, 5 mM $MgCl_2$, 10 μg ml^{-1} BSA, 10 μg ml^{-1} tRNA, 0.05% Igepal CA-630 and 5% glycerol) with a 100-fold molar excess of C2c2 relative to 5′-labelled pre-crRNA (final concentrations of 100 nM and <1 nM, respectively). Unless otherwise indicated, the reaction was quenched after 1 h with 1.5× RNA loading dye (100% formamide, 0.025% (w/v) bromophenol blue and 200 μg ml^{-1} heparin). After quenching, reactions were denatured at 95 °C for 5 min before resolving by 12% or 15% denaturing PAGE (0.5× TBE buffer). Metal dependence of the reaction was tested by addition of EDTA or EGTA to the reaction buffer at concentrations varying from 10 to 100 mM. Bands were visualized by phosphorimaging and quantified with ImageQuant (GE Healthcare). The percentage cleavage was determined as the ratio of the product band intensity to the total intensity of both the product and uncleaved pre-crRNA bands and normalized for background within each measured substrate using ImageQuant TL Software (GE Healthcare) and fit to a one phase exponential association using Prism (GraphPad).

Product size mapping and 3′ end moiety identification. Cleavage product length was determined biochemically by comparing gel migration of product bands to alkaline hydrolysis and RNase T1 digestion ladders using the RNase T1 Kit from Ambion. For the hydrolysis ladder, 15 nM full-length RNA substrates were incubated at 95 °C in 1× alkaline hydrolysis buffer (Ambion) for 5 min. Reactions were quenched with 1.5× RNA loading buffer, and cooled to −20 °C to immediately stop hydrolysis. For the RNase T1 ladder, 15 nM full-length RNA substrates were unfolded in 1× RNA sequencing buffer (Ambion) at 65 °C. Reactions were cooled to ambient temperature, and then 1 U of RNase T1 (Ambion) was added to reaction. After 15 min, reactions were stopped by phenol–chlorofrom extraction and 1.5× RNA loading buffer was added for storage. Hydrolysis bands were resolved in parallel to cleavage samples on 15% denaturing PAGE and visualized by phosphorimaging. For 3′ end moiety identification, products from the processing reaction were incubated with 10 U of T4 polynucleotide kinase (New England Biolabs) for 1 h at 37 °C in processing buffer. Reactions were quenched with 1.5× RNA loading buffer, resolved on 20% denaturing PAGE and visualized by phosphorimaging.

Small RNA sequencing analysis. RNA reads from ref. 10 were downloaded from SRA runs SRR3713697, SRR3713948 and SRR3713950. The paired-end reads were locally mapped to the reference sequences using Bowtie2 (ref. 34) with the following options: "-reorder-very-fast-local-local". The mapping was then filtered to retain only alignments that contained no mismatch using mapped.py (https://github.com/christophertbrown/mapped) with the "-m 0 -p both" options. BAM files of the resulting mapping are in the Supplementary Information. Read coverage was visualized using Geneious and plotted using Prism (GraphPad).

Target cleavage assays. Target cleavage assays were performed at 25 °C or 37 °C in cleavage buffer (20 mM HEPES pH 6.8, 50 mM KCl, 5 mM $MgCl_2$ and 5% glycerol). crRNA guides were pre-folded by heating to 65 °C for 5 min and then slowly cooling to ambient temperature in cleavage buffer. C2c2–crRNA complex formation was performed in cleavage buffer, generally at a molar ratio of 2:1 protein to crRNA at 37 °C for 10 min, before adding 5′-end labelled target and/or other non-radiolabelled RNA target substrates. Unless otherwise indicated, final concentrations of protein, guide and targets were 100 nM, 50 nM and <1 nM, respectively, for all reactions. Reactions were quenched with 1.5× RNA loading dye and resolved by 15% denaturing PAGE (0.5× TBE buffer). Bands were visualized by phosphorimaging and quantified with ImageQuant (GE Healthcare). The percentage cleavage was determined as the ratio of total banding intensity for all shorter products relative to the uncleaved band and normalized for background within each measured substrate using ImageQuant TL Software (GE Healthcare) and fit to a one phase exponential association using Prism (GraphPad).

crRNA filter-binding assays. Filter binding assays were carried out in RNA processing buffer (20 mM HEPES pH 6.8, 50 mM KCl, 5 mM $MgCl_2$, 10 μg ml^{-1} BSA, 10 μg ml^{-1} yeast tRNA, 0.01% Igepal CA-630 and 5% glycerol). LbuC2c2 was incubated with radiolabelled crRNA (<0.1 nM) for 1 h at 37 °C. Tufryn, Protran and Hybond-N + were assembled onto a dot-blot apparatus in the order listed above. The membranes were washed twice with 50 μl equilibration buffer (20 mM HEPES pH 6.8, 50 mM KCl, 5 mM $MgCl_2$ and 5% glycerol) before the sample was applied to the membranes. Membranes were again washed with 50 μl equilibration buffer, dried and visualized by phosphorimaging. Data were quantified with ImageQuant TL Software (GE Healthcare) and fit to a binding isotherm using Prism (GraphPad Software). All experiments were carried out in triplicate. Dissociation constants and associated errors are reported in the figure legends.

Electrophoretic mobility-shift assays. To avoid the dissociation of the LbuC2c2-dHEPN1/dHEPN2–crRNA complex at low concentrations during ssRNA-binding experiments, binding reactions contained a constant excess of LbuC2c2-dHEPN1/dHEPN2 (200 nM), and increasing concentrations of crRNA-A and <0.1 nM target ssRNA. Assays were carried out in C2c2 EMSA buffer (20 mM HEPES pH 6.8, 50 mM KCl, 10 μg ml^{-1} BSA, 100 μg ml^{-1} yeast tRNA, 0.01% Igepal CA-630 and 5% glycerol). LbuC2c2–crRNA-A complexes were pre-formed as described above for 10 min at 37 °C before the addition of 5′-radiolabelled ssRNA substrate and a further incubation for 45 min at 37 °C. Samples were then resolved by 8% native PAGE at 4 °C (0.5× TBE buffer). Gels were imaged by phosphorimaging, quantified using ImageQuant TL Software (GE Healthcare) and fit to a binding isotherm using Prism (GraphPad Software). All experiments were carried out in triplicate. Dissociation constants and associated errors are reported in the figure legends.

Fluorescent RNA detection assay. LbuC2c2–crRNA complexes were preassembled by incubating 1 μM of LbuC2c2 with 500 nM of crRNA for 10 min at 37 °C. These complexes were then diluted to 100 nM LbuC2c2, 50 nM crRNA, in RNA processing buffer (20 mM HEPES pH 6.8, 50 mM KCl, 5 mM $MgCl_2$, 10 μg ml^{-1} BSA, 10 μg ml^{-1} yeast tRNA, 0.01% Igepal CA-630 and 5% glycerol) in the presence of 185 nM of RNAase-Alert substrate (Thermo-Fisher), 100 ng of HeLa total RNA and increasing amounts of target 60-nucleotide ssRNA (0–1 nM). These reactions were incubated in a fluorescence plate reader (Tecan Infinite Pro F200) for up to 120 min at 37 °C with fluorescence measurements taken every 5 min (λ_{ex}: 485 nm; λ_{em}: 535 nm). Background-corrected fluorescence values were obtained by subtracting fluorescence values obtained from reactions carried out in the absence of target ssRNA. Maximal fluorescence was measured by incubating 50 nM RNase A with 185 nM of RNAase-Alert substrate. For measurement of crRNA-*ACTB*-mediated LbuC2c2 activation by β-actin mRNA in human total RNA, LbuC2c2–crRNA complexes were preassembled by incubating 1 μM of LbuC2c2 with 500 nM of crRNA-*ACTB* for 10 min at 37 °C and reactions were carried out in the conditions above in the presence of increasing amounts (0–1 μg) of either HeLa cell total RNA or *E. coli* total RNA (as a negative control). These reactions were incubated in a fluorescence plate reader for up to 180 min at 37 °C with fluorescence measurements taken every 5 min (λ_{ex}: 485 nm; λ_{em}: 535 nm). Background-corrected fluorescence

© 2016 Macmillan Publishers Limited, part of Springer Nature. All rights reserved.

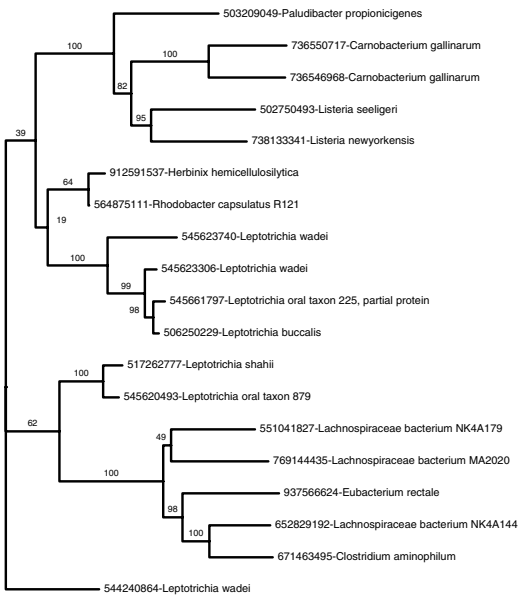
values were obtained by subtracting fluorescence values obtained from reactions carried out in the absence of target ssRNA. For coupled pre-crRNA processing and RNA detection assays, LbuCas9–crRNA complexes were preassembled by incubating 1 μM of LbuC2c2 with 500 nM of pre-crRNA-A-λ2 for 20 min at 37 °C and reactions carried out as described above in the presence of increasing amounts of ssRNA A and ssRNA λ2 (0–1 nM each). In each case, error bars represent the standard deviation from three independent experiments.

Background cleavage in total RNA. LbuC2c2–crRNA-λ4 complexes were assembled as previously described for fluorescence RNA detection assay. Complexes were incubated in RNA processing buffer in the presence of 3 μg total RNA with and without 10 nM λ4 ssRNA target. After 2 h, RNA was isolated by trizol extraction and ethanol precipitation. The RNA fragment size distribution of resuspended samples was resolved using Small RNA Analysis Kit (Agilent) on a Bioanalyzer 2100 (Agilent) using the manufacturer's protocol. Fluorescent intensity curves were normalized in Prism for curve overlay (GraphPad Software).

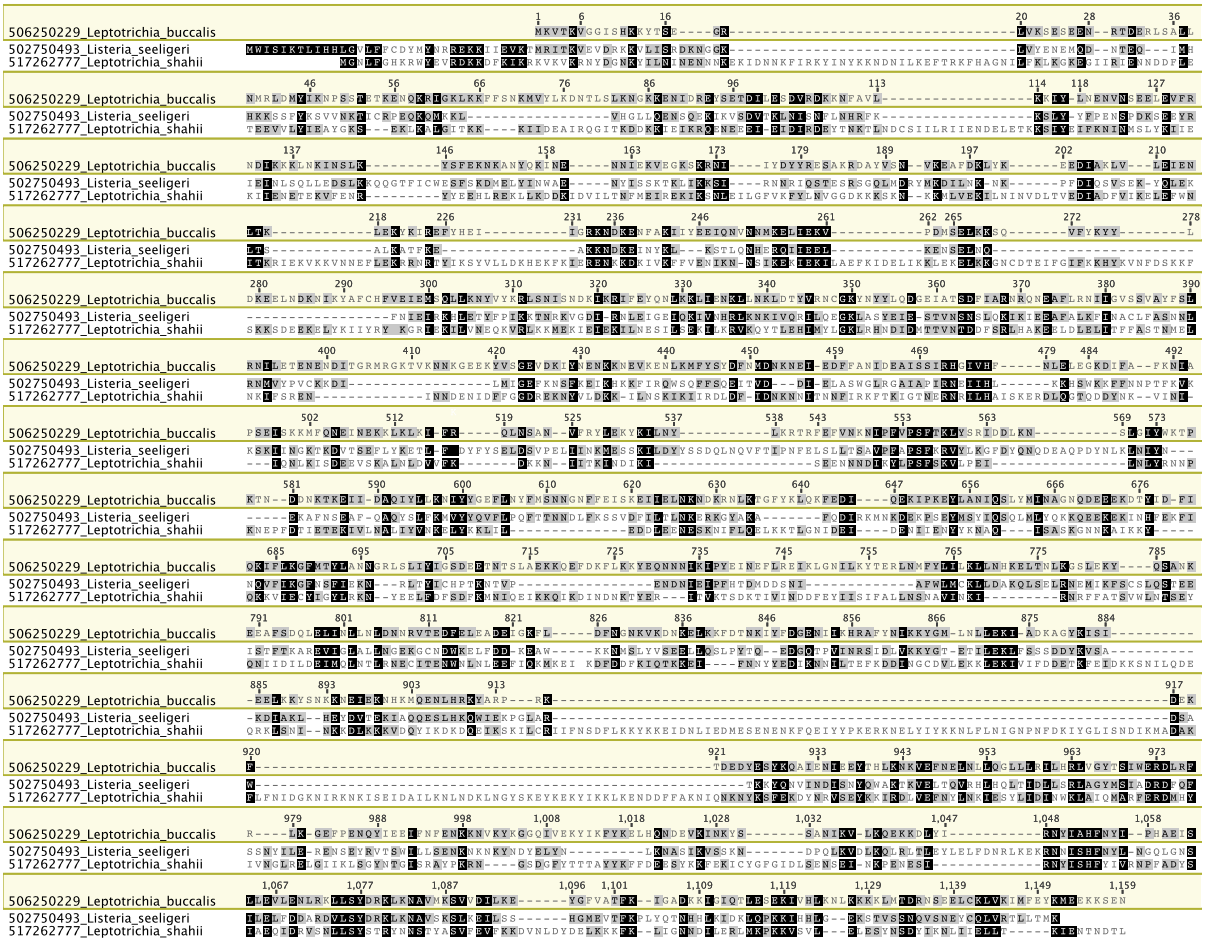
31. Stamatakis, A. RAxML version 8: a tool for phylogenetic analysis and post-analysis of large phylogenies. *Bioinformatics* **30,** 1312–1313 (2014).
32. Katoh, K. & Standley, D. M. MAFFT multiple sequence alignment software version 7: improvements in performance and usability. *Mol. Biol. Evol.* **30,** 772–780 (2013).
33. Sternberg, S. H., Haurwitz, R. E. & Doudna, J. A. Mechanism of substrate selection by a highly specific CRISPR endoribonuclease. *RNA* **18,** 661–672 (2012).
34. Langmead, B. & Salzberg, S. L. Fast gapped-read alignment with Bowtie 2. *Nat. Methods* **9,** 357–359 (2012).

© 2016 Macmillan Publishers Limited, part of Springer Nature. All rights reserved.

a

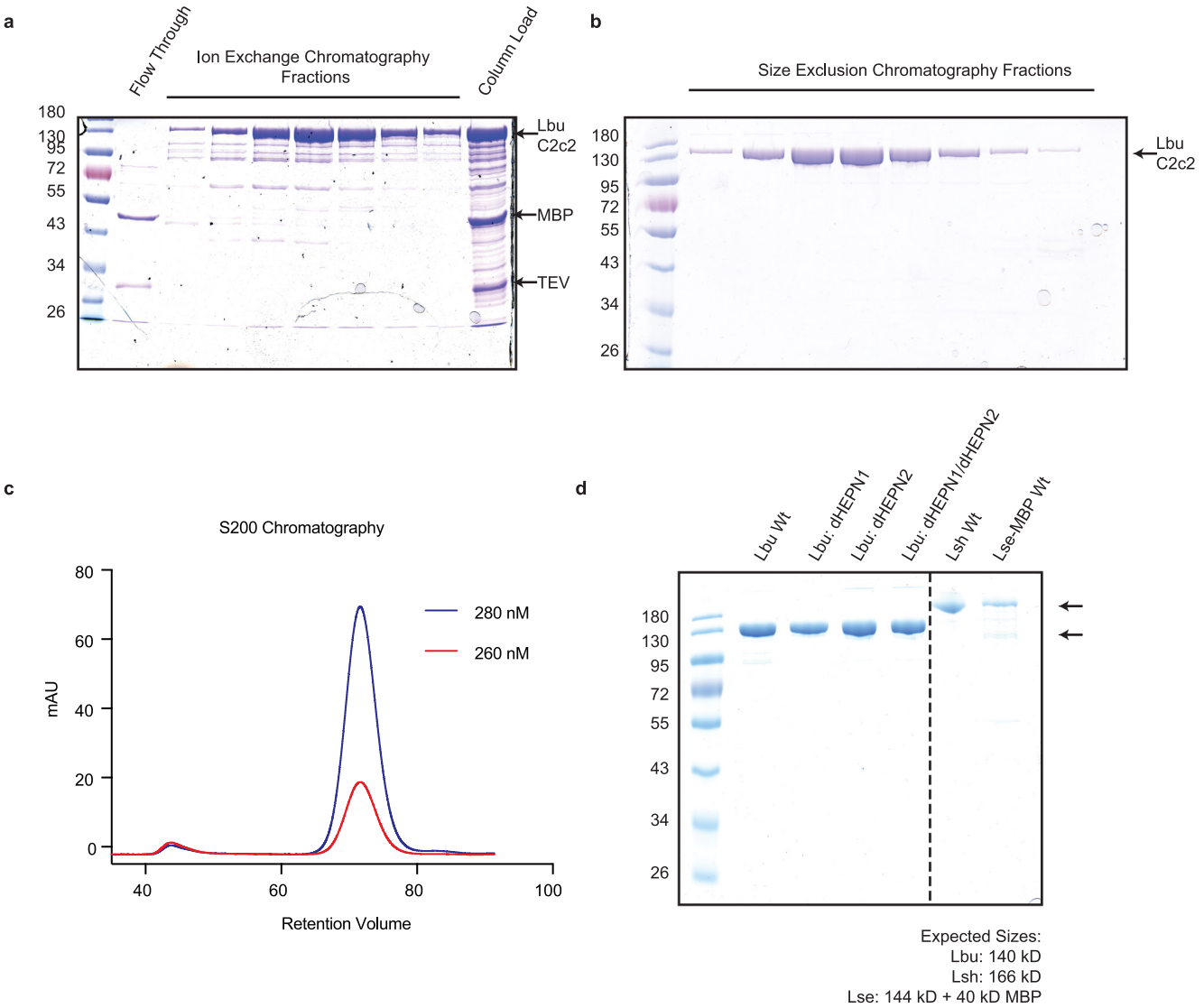


b



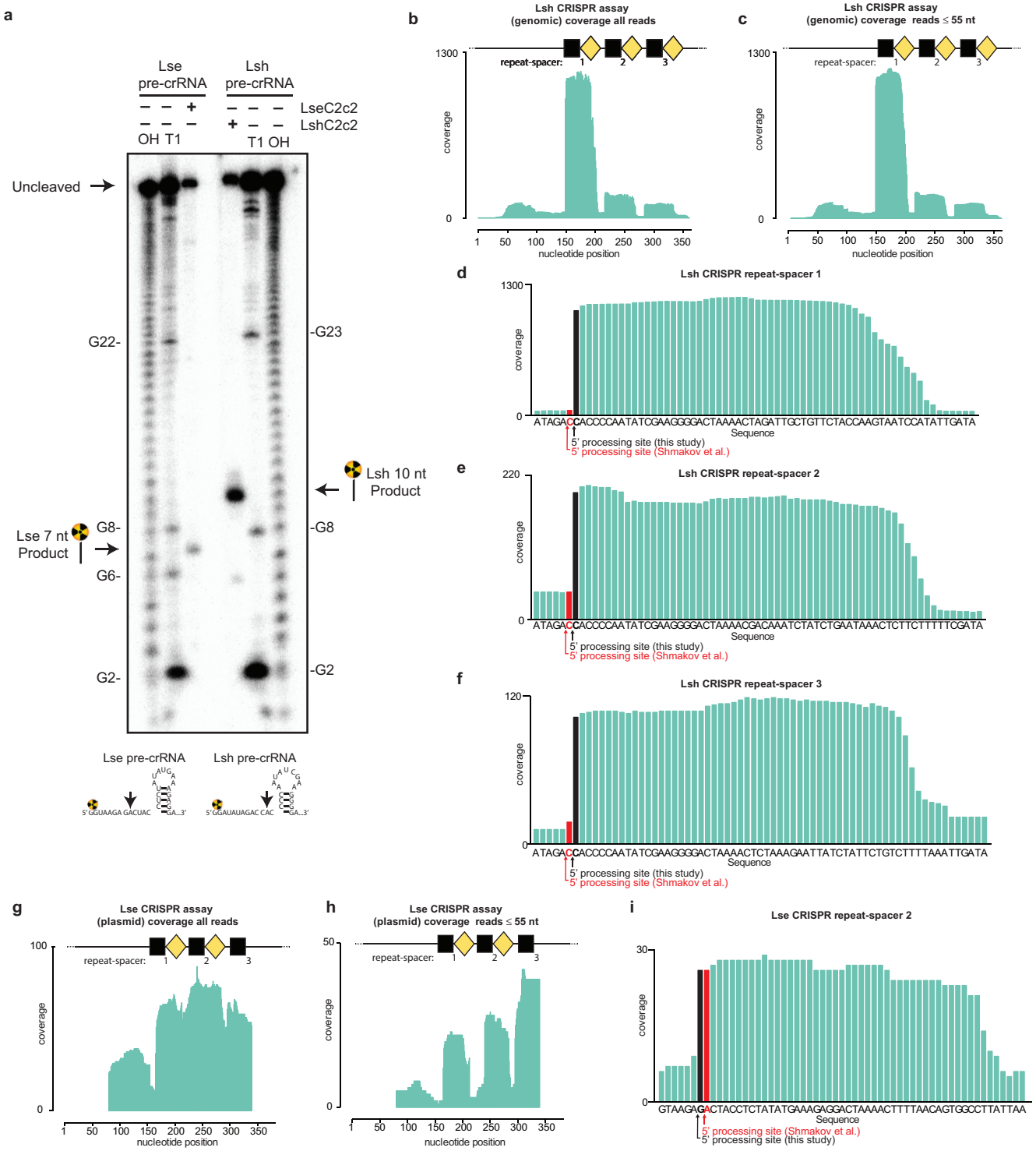
Extended Data Figure 1 | Complete phylogenetic tree of C2c2 family and C2c2 alignment. a, Maximum-likelihood phylogenetic reconstuction of C2c2 proteins. Leaves include GI protein numbers and organism of origin; bootstrap support values, out of 100 resamplings, are presented for inner split. Scale is in substitutions per site. **b**, Multiple sequence alignment of the three analysed homologues of C2c2; coordinates are based on LbuC2c2.

© 2016 Macmillan Publishers Limited, part of Springer Nature. All rights reserved.



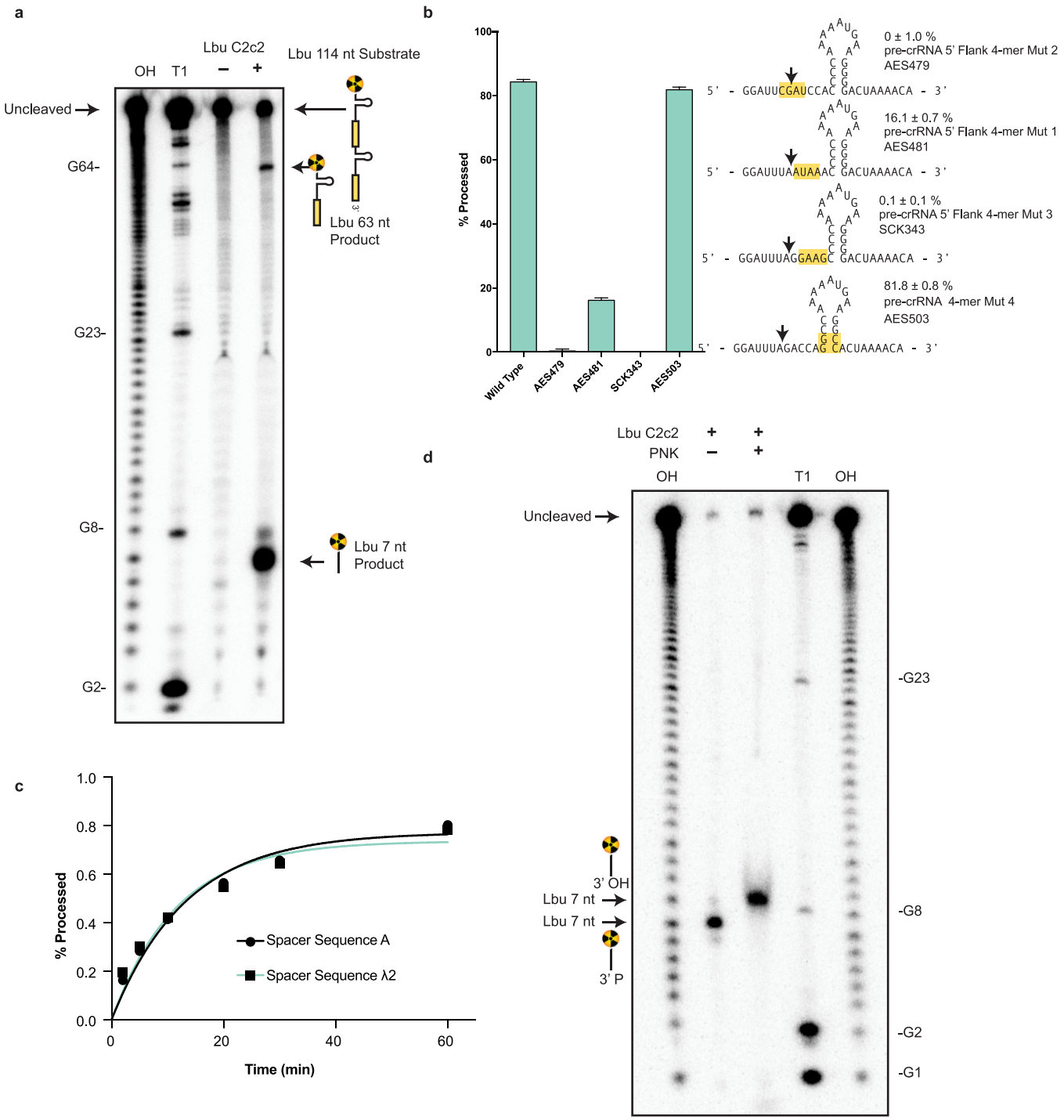
Extended Data Figure 2 | Purification and Production of C2c2. All C2c2 homologues were expressed in *E. coli* as His-MBP fusions and purified by a combination of affinity, ion exchange and size exclusion chromatography. The Ni^{+} affinity tag was removed by incubation with TEV protease. **a**, **b**, Representative SDS–PAGE gels of chromatography fractions are shown. **c**, The chromatogram from Superdex 200 (16/60) column demonstrating that C2c2 elutes as a single peak, devoid of nucleic acid. **d**, SDS–PAGE analysis of purified proteins used.

© 2016 Macmillan Publishers Limited, part of Springer Nature. All rights reserved.



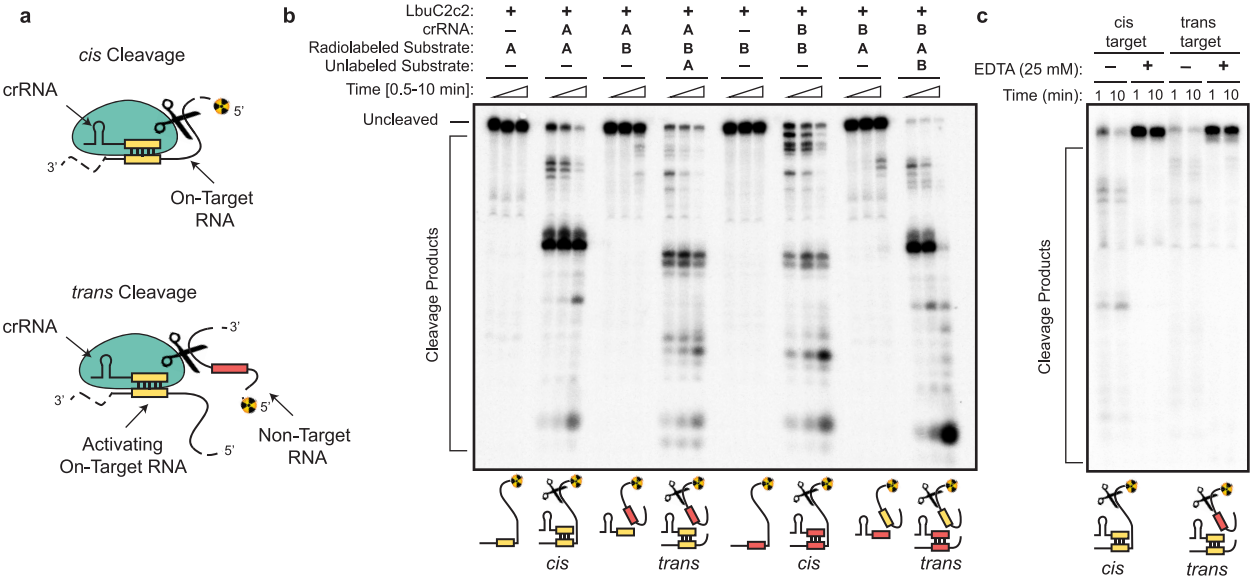
Extended Data Figure 3 | Mapping of pre-crRNA processing by C2c2 *in vitro* and *in vivo*. **a**, Cleavage site mapping of LseC2c2 and LshCc2c2 cleavage of a single cognate pre-crRNA array. Cleavage reactions were performed with 100 nM C2c2 and <1 nM pre-crRNA. **b**–**i**, Re-analysis of LshC2c2 (**b**–**f**) and LseC2c2 (**g**–**i**) CRISPR array RNA sequencing experiments from ref. 10 (supplementary figs S7 and S5 of ref. 10, respectively). All reads (**b**, **g**) and filtered reads (55 nucleotides or less; as per original analysis[10]; **c**, **h**) were stringently aligned to each CRISPR array using Bowtie2 (see Methods). Detailed views of individual CRISPR repeat-spacers are shown for Lsh (**d**–**f**) and Lse (**i**). Differences in 5′ end pre-crRNA processing are indicated by arrows below each sequence. BAM alignment files of our analysis are available in Supplementary Information. This mapping clearly indicates that the 5′ ends of small RNA sequencing reads generated from Lsh pre-crRNAs map to a position 2 nucleotides from the base of the predicted hairpin, in agreement with our *in vitro* processing data (**a**). This pattern holds for all mature crRNAs detected from both native expression in *L. shahii* and heterologous expression in *E. coli* (data not shown, BAM file available in Supplementary Information). Unfortunately, the LseC2c2 crRNA sequencing data (used in **g**–**i**) is less informative owing to low read depth, and each aligned crRNA exhibits a slightly different 5′ end with little obvious uniformity. The mapping for one of the processed repeats (repeat-spacer 2; **i**) is in agreement with our data but only with low confidence due to the insufficient read depth.

© 2016 Macmillan Publishers Limited, part of Springer Nature. All rights reserved.



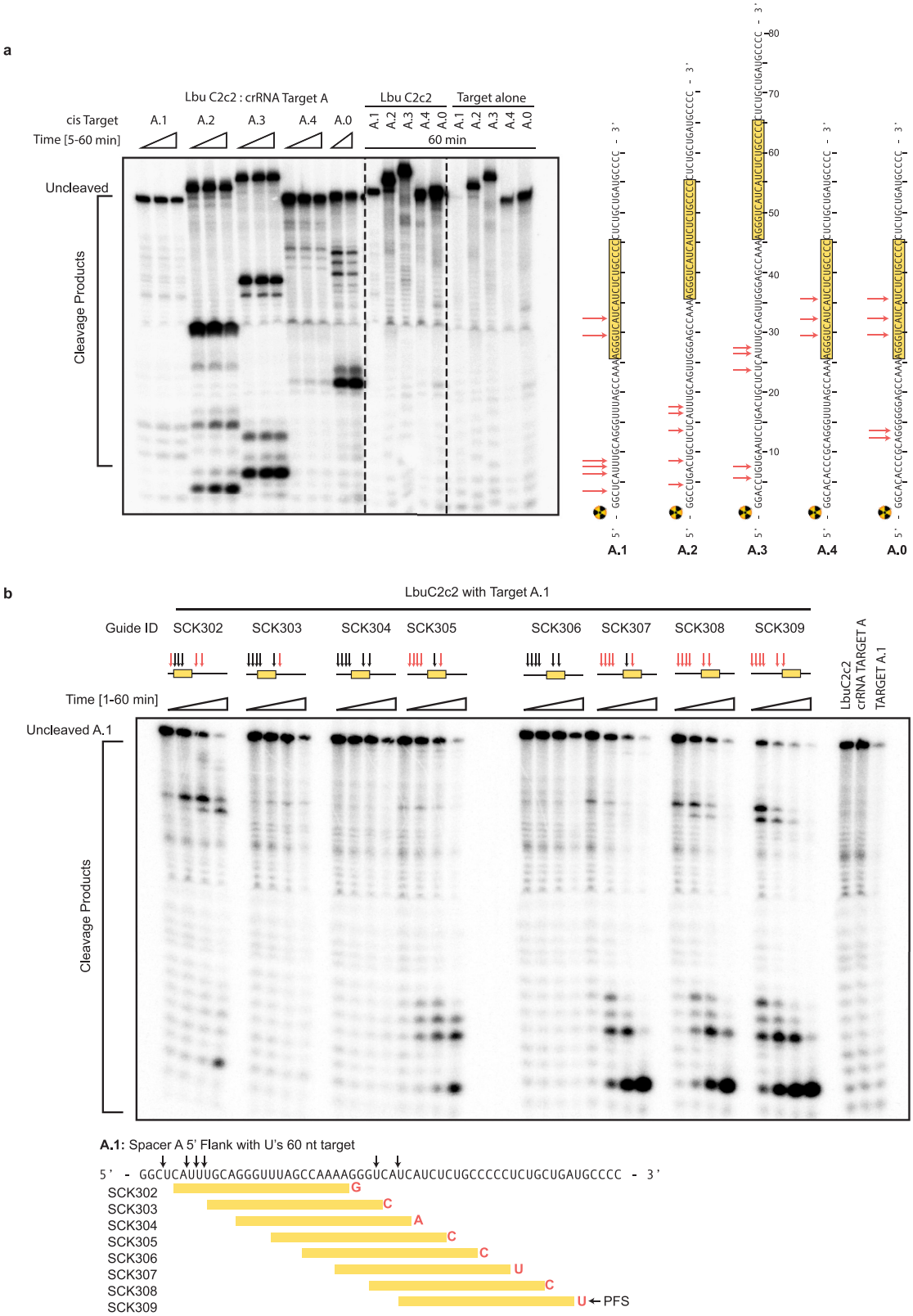
Extended Data Figure 4 | Pre-crRNA processing by C2c2 is spacer-sequence independent, can occur on tandem crRNA arrays, is affected by mutations in the 5′ flanking region of the pre-cRNA and produces a 3′ phosphate product. a, Cleavage site mapping of LbuC2c2 cleavage of a tandem pre-crRNA array. Cleavage reactions were performed with 100 nM LbuC2c2 and <1 nM pre-crRNA. A schematic of cleavage products is depicted on right, with arrows indicating the mapped C2c2 cleavage products. **b**, LbuC2c2 4-mer mutant pre-crRNA processing data demonstrating the importance of the 5′ single-stranded flanking region for efficient pre-crRNA processing. Percentage of pre-crRNA processing was measured after 1 h (mean ± s.d., $n = 3$). **c**, Representative LbuC2c2 pre-crRNA cleavage time course demonstrating that similar rates of pre-crRNA processing occur independent of crRNA spacer sequence pseudo-first-order rate constants (k_{obs}) (mean ± s.d.) are $0.07 \pm 0.04\ min^{-1}$ and $0.08 \pm 0.04\ min^{-1}$ for spacer A and spacer λ2, respectively. **d**, End group analysis of cleaved RNA by T4 polynucleotide kinase (PNK) treatment. Standard processing assay conditions were used to generate cleavage product, which was then incubated with PNK for 1 h to remove any 2′,3′-cyclic phosphates/3′ monophosphates. Retarded migration of band indicates removal of the charged, monophosphate from the 3′ end of radiolabelled 5′ product.

© 2016 Macmillan Publishers Limited, part of Springer Nature. All rights reserved.



Extended Data Figure 5 | LbuC2c2 catalyses guide-dependent ssRNA degradation on *cis* and *trans* targets. a, Schematic of the two modes of C2c2, guide-dependent ssRNA degradation. **b**, Cleavage of two distinct radiolabelled ssRNA substrates, A and B, by LbuC2c2. Complexes of 100 nM C2c2 and 50 nM crRNA were pre-formed at 37 °C, and reaction was initiated upon addition of <1 nM 5′-labelled target RNA at 25 °C. *Trans* cleavage reactions contained equimolar (<1 nM) concentrations of radiolabelled non-guide-complementary substrate, and unlabelled on-target ssRNA. For multiple ssRNA substrates, we observed that LbuC2c2 catalysed efficient cleavage only when bound to the complementary crRNA, indicating that LbuC2c2–crRNA cleaves ssRNA in an RNA-guided fashion. This activity is hereafter referred to as on-target or *cis*-target cleavage. LbuC2c2-mediated *cis* cleavage resulted in a laddering of multiple products, with cleavage preferentially occurring before uracil residues, analogous to LshC2c2 (ref. 9). We repeated non-target cleavage reactions in the presence of unlabelled, on-target (crRNA-complementary) ssRNA. In contrast to non-target cleavage experiments performed in *cis*, we observed rapid degradation of non-target RNA in *trans*. The similar RNA cleavage rates and near-identical cleavage products observed for both *cis* on-target cleavage and *trans* non-target cleavage implicate the same nuclease centre in both activities. **c**, LbuC2c2 loaded with crRNA targeting spacer A was tested for cleavage activity under both *cis* (target A labelled) and *trans* (target B labelled in the presence of unlabelled target A) cleavage conditions in the presence of 25 mM EDTA.

© 2016 Macmillan Publishers Limited, part of Springer Nature. All rights reserved.

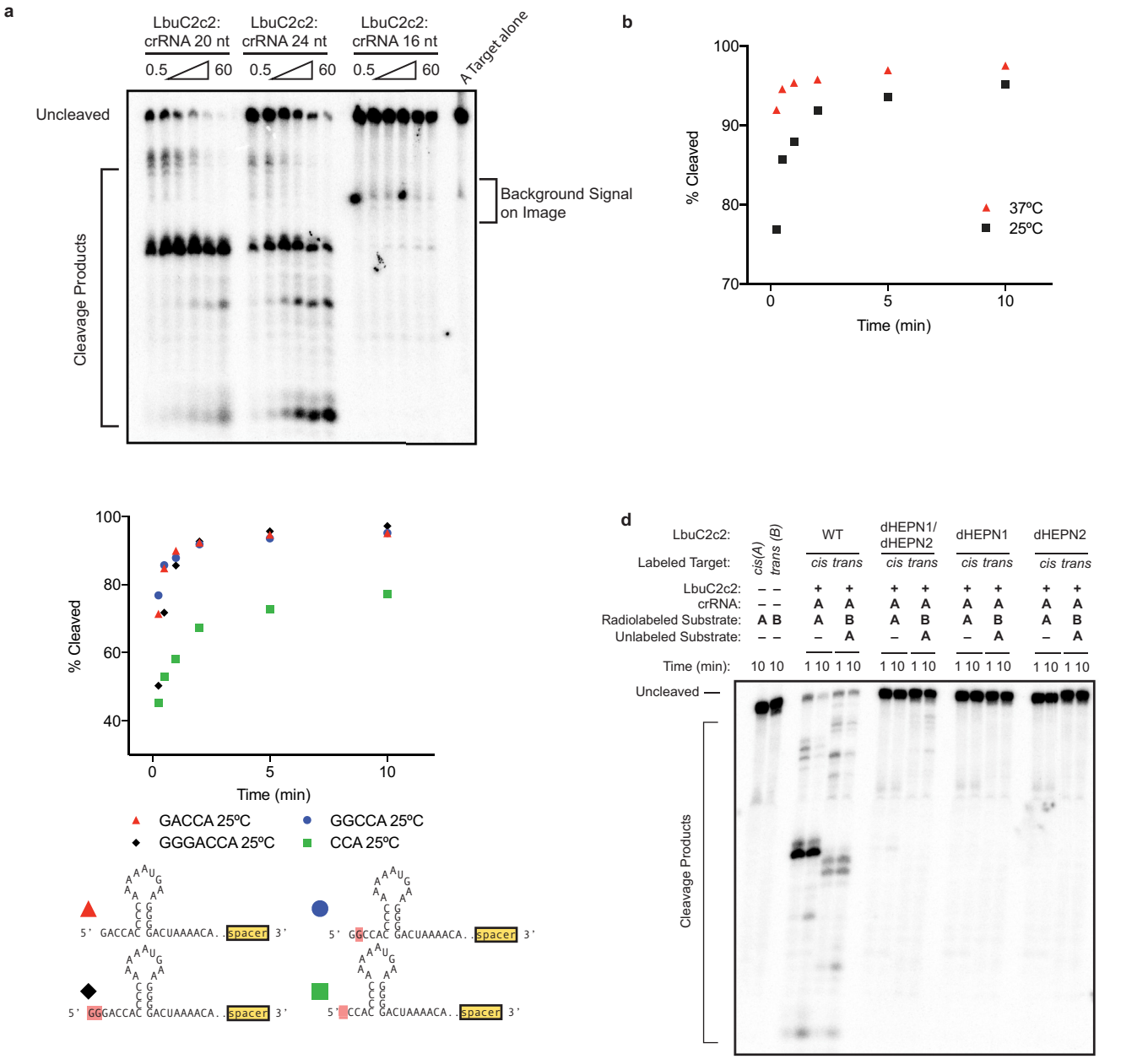


Extended Data Figure 6 | See next page for caption.

© 2016 Macmillan Publishers Limited, part of Springer Nature. All rights reserved.

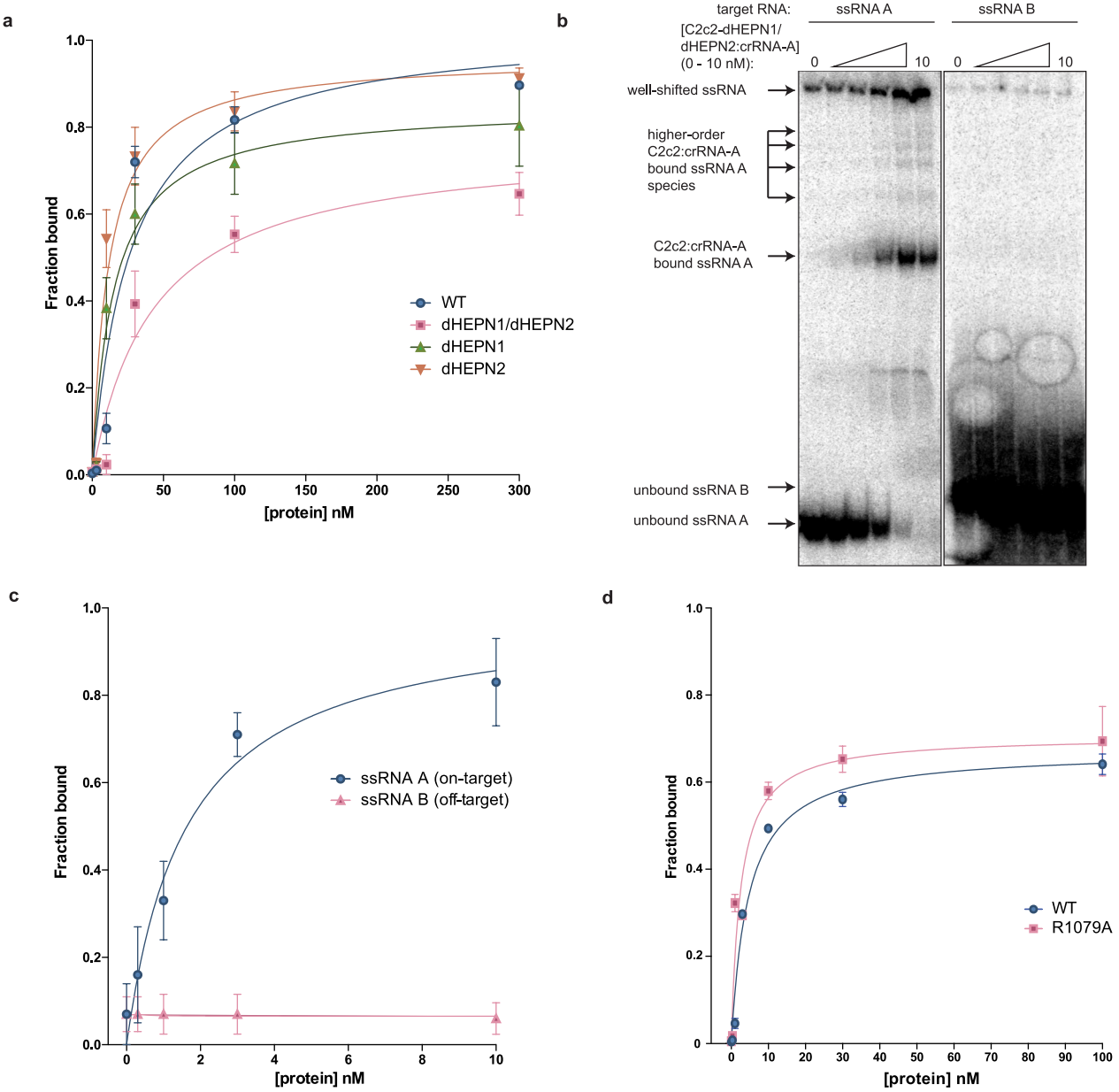
Extended Data Figure 6 | LbuC2c2 ssRNA target cleavage site mapping. **a**, ssRNA target cleavage assay conducted per Methods demonstrating LbuC2c2-mediated '*cis*' cleavage of several radiolabelled ssRNA substrates with identical spacer-complementary sequences but distinct 5′ flanking sequences of variable length and nucleotide composition. Sequences of ssRNA substrates are shown to the right with spacer-complementary sequences for crRNA-A highlighted in yellow. Arrows indicate detected cleavage sites. Gel was cropped for clarity. It should be noted that the pattern of cleavage products produced on different substrates (for example, A.1 versus A.2 versus A.3) indicates that the cleavage site choice is primarily driven by a uracil preference and exhibits an apparent lack of exclusive cleavage mechanism within the crRNA-complementary target sequence, which is in contrast to what is observed for other class II CRISPR single effector complexes such as Cas9 and Cpf1 (refs 11, 21). Notably, the cleavage pattern observed for substrate A.0 hints at a secondary preference for polyG sequences. **b**, LbuC2c2 ssRNA target cleavage assay as per Methods, using a range of crRNAs that tile the length of the ssRNA target. The sequence of the ssRNA substrates used in this experiment is shown below the gel with spacer-complementary sequences for each crRNA highlighted in yellow. Arrows indicate predicted cleavage sites. Above each set of lanes, a small diagram indicates the location of the spacer sequence along the target (yellow box) and the cleavage products observed (red arrows) or absent (black arrows). Likewise, it should be noted that for every crRNA the cleavage product length distribution is very similar, again indicating an apparent lack of exclusive cleavage within the crRNA-bound sequence. The absence of a several cleavage products in a subset of the reactions might be explained by the presence of bound C2c2–crRNA on the ssRNA target, which could sterically occlude access to uracils by any *cis* (intramolecular) or *trans* (intermolecular) LbuC2c2 active sites. While proper analysis for protospacer flanking site (PFS) preference for LbuC2c2 is beyond the scope of this study, minimal impact of the 3′ flanking nucleotide was observed. Expected PFS base is noted in diagram next to each guide tested in red.

© 2016 Macmillan Publishers Limited, part of Springer Nature. All rights reserved.



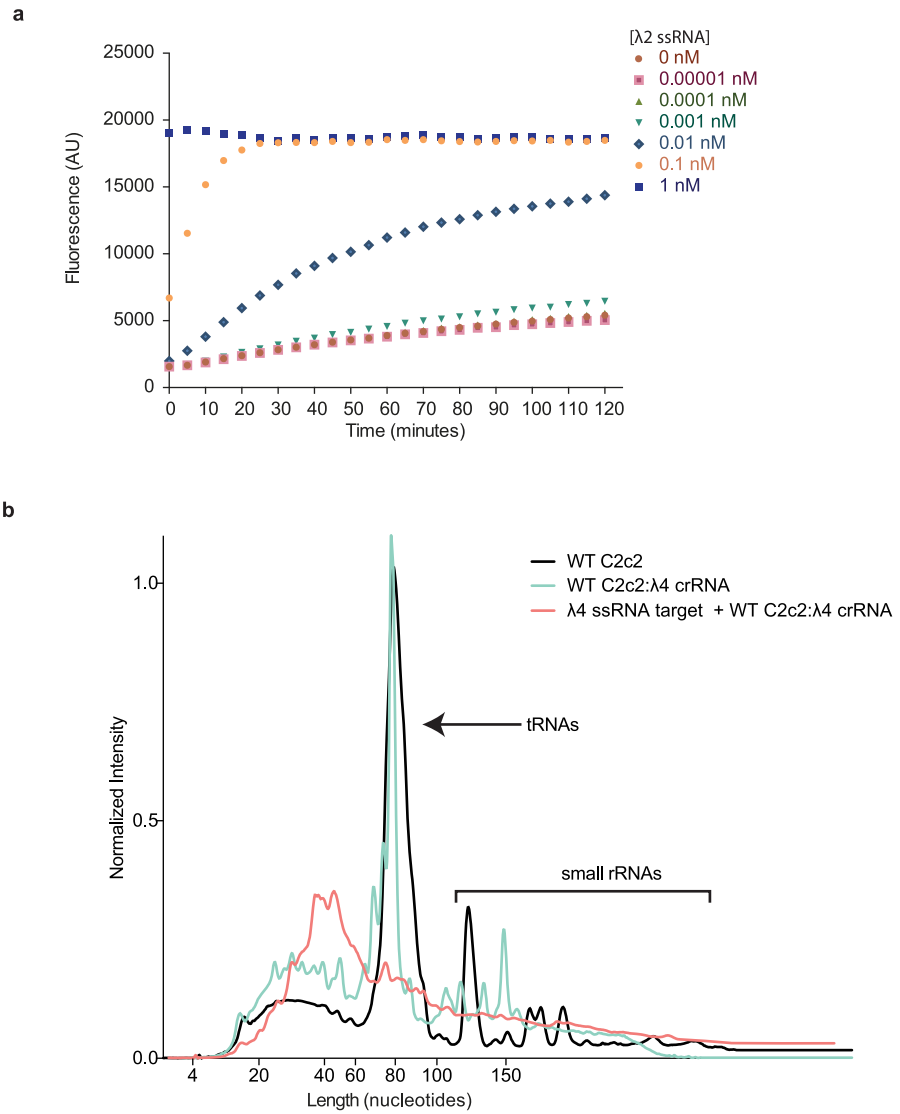
Extended Data Figure 7 | Dependence of RNA targeting on crRNA variants, temperature and point mutations. a, LbuC2c2 ssRNA target cleavage assay carried out, as per Methods with crRNAs possessing 16-, 20- or 24-nucleotide spacers. **b**, LbuC2c2 ssRNA target cleavage time-course carried out at either 25 °C or 37 °C as per the Methods. **c**, LbuC2c2 ssRNA target cleavage time course carried out as stated in the Methods with crRNAs possessing different 5′-flanking nucleotide mutations. Mutations are highlighted in red. One- to two-nucleotide 5′ extensions negligibly impacted cleavage efficiencies. By contrast, shortening the flanking region to 3 nucleotides slowed cleavage rates. **d**, Effect of point mutations on RNase activity of C2c2 in conserved residue mutants within HEPN motifs for ssRNA targeting.

© 2016 Macmillan Publishers Limited, part of Springer Nature. All rights reserved.



Extended Data Figure 8 | Binding data for LbuC2c2 to mature crRNA and target ssRNA. a, Filter binding assays were conducted as described in the Methods to determine the binding affinity of mature crRNA-A_GG to LbuC2c2-WT, LbuC2c2-dHEPN1, LbuC2c2-dHEPN2, or LbuC2c2-dHEPN1/dHEPN2. The quantified data were fit to standard binding isotherms. Error bars represent the s.d. from three independent experiments. Measured dissociation constants from three independent experiments (mean ± s.d.) were 27.1 ± 7.5 nM (LbuC2c2-WT), 15.2 ± 3.2 nM (LbuC2c2-dHEPN1), 11.5 ± 2.5 nM (LbuC2c2-dHEPN2), and 43.3 ± 11.5 nM (LbuC2c2-dHEPN1/dHEPN2). **b**, Representative electrophoretic mobility shift assay for binding reactions between LbuC2c2-dHEPN1/dHEPN2: crRNA-A_GG and either 'on-target' A ssRNA or 'off-target' B ssRNA, as indicated. Three independent experiments were conducted as described in the Methods. The gel was cropped for clarity. **c**, Quantified binding data from **b** were fitted to standard binding isoforms. Error bars represent the s.d. from three independent experiments. Measured dissociation constants from three independent experiments (mean ± s.d.) were 1.62 ± 0.43 nM for ssRNA A and not determined (N.D.;>>10 nM) for ssRNA B. **d**, Filter binding assays were conducted as described in the Methods to determine the binding affinity of mature crRNA-A_GA to LbuC2c2-WT and LbuC2c2-R1079A. The quantified data were fit to standard binding isotherms. Error bars represent the s.d. from three independent experiments. Measured dissociation constants from three independent experiments (mean ± s.d.) were 4.65 ± 0.6 nM (LbuC2c2-WT) and 2.52 ± 0.5 nM (LbuC2c2-R1079A). It is of note that these binding affinities differ from **a**. This difference is accounted for in a slight difference in the 5′ sequence of the guide with panel **a** guides beginning with a 5′-G**(G)**CCA… and panel d 5`-G**(A)**CCA. While the native sequence guide (5′-G**(A)**CCA) binds tighter to LbuC2c2, no difference is seen in the RNA targeting efficiencies of these guide variants (Extended Data Fig. 6c).

© 2016 Macmillan Publishers Limited, part of Springer Nature. All rights reserved.



Extended Data Figure 9 | RNase detection assay λ2-ssRNA time course. a, LbuC2c2:crRNA-λ2 was incubated with RNAase-Alert substrate (Thermo-Fisher) and 100 ng HeLa total RNA in the presence of increasing amounts of λ2 ssRNA (0-1 nM) for 2 h at 37 °C. Fluorescence measurements were taken every 5 min. The 1 nM λ2 ssRNA reaction reached saturation before the first time point could be measured. Error bars represent the s.d. from three independent experiments. **b**, LbuC2c2–crRNA-λ4 or apo LbuC2c2 was incubated in HeLa total RNA for 2 h in the presence or absence of on-target activating λ4 ssRNA. Degradation of background small RNA was resolved on a small RNA chip in a Bioanalyzer 2100 as described in the Methods. Small differences are seen in the fragment profile of between apo LbuC2c2 and LbuC2c2:crRNA-λ4. By contrast, upon addition of the on-target ssRNA to the reaction, a notable broadening and shifting of the tRNA peak reveals extensive degradation of other structured and nonstructured RNA's present in the reaction upon activation of LbuC2c2 *trans* activity.

© 2016 Macmillan Publishers Limited, part of Springer Nature. All rights reserved.

Extended Data Table 1 | Oligonucleotides used in this study

Name	Sequence	Used in
Lbu_pre-crRNA_A_SCK314	5'-GGAUUUAGACCACCCCAAAAAUGAAGGGGACUAAAACAGGGGCAGAGAUGAUGACCCU-3'	Fig. 1c, 2a-c, 3a,c, ED3
Lse_pre-crRNA_B_AES484	5'-GGUAAGAGACUACCUCUAUAUGAAAGAGGACUAAAACCAAACAUGAUCUGGGUCAUC-3'	Fig. 1c, ED3
Lsh_pre-crRNA_A_SCK339	5'-GGAUUUAGACCACCCCAAUAUCGAAGGGGACUAAAACAGGGGCAGAGAUGAUGACCCU-3'	Fig. 1c. ED3
Lbu_pre-crRNA_invert_SCK321	5'-GGAUUUAGACCAGGGGAAGUAAAAACCCCACUAAAACAGGGGCAGAGAUGAUGACCCU-3'	Fig. 2a
Lbu_pre-crRNA_5stem_SCK331	5'-GGAUUUAGACCACCCCCAAAAAUGAAGGGGGACUAAAACAGGGGCAGAGAUGAUGACCCU-3'	Fig. 2a
Lbu_pre-crRNA_7bubble_SCK334	5'-GGAUUUAGACCACCCCAUGAAGGGGACUAAAACAGGGGCAGAGAUGAUGACCCU-3'	Fig. 2a
Lbu_pre-crRNA_5bubble_SCK335	5'-GGAUUUAGACCACCCCAUGAAGGGGACUAAAACAGGGGCAGAGAUGAUGACCCU-3'	Fig. 2a
Lbu_pre-crRNA_3stem_SCK342	5'-GGAUUUAGACCACCCCAAAAAUGAAGGGCACUAAAACAGGGGCAGAGAUGAUGACCCU-3'	Fig. 2a
Lbu_pre-cr_5'_mut1_AES497	5'-GGCGUUAGACCACCCCAAAAAUGAAGGGGACUAAAACAGGGGCAGAGAUGAUGACCCU-3'	Fig. 2b, ED4
Lbu_pre-cr_5'_mut2_AES496	5'-GGAGCUAGACCACCCCAAAAAUGAAGGGGACUAAAACAGGGGCAGAGAUGAUGACCCU-3'	Fig. 2b, ED4
Lbu_pre-cr_5'_mut3_AES495	5'-GGAUCCAGACCACCCCAAAAAUGAAGGGGACUAAAACAGGGGCAGAGAUGAUGACCCU-3'	Fig. 2b, ED4
Lbu_pre-cr_5'_mut4_AES477	5'-GGAUUCGGACCACCCCAAAAAUGAAGGGGACUAAAACAGGGGCAGAGAUGAUGACCCU-3'	Fig. 2b, ED4
Lbu_pre-cr_5'_mut5_AES482	5'-GGAUUUACCCCACCCCAAAAAUGAAGGGGACUAAAACAGGGGCAGAGAUGAUGACCCU-3'	Fig. 2b, ED4
Lbu_pre-cr_5'_mut6_AES478	5'-GGAUUUAAUCCACCCCAAAAAUGAAGGGGACUAAAACAGGGGCAGAGAUGAUGACCCU-3'	Fig. 2b, ED4
Lbu_pre-cr_5'_mut7_AES480	5'-GGAUUUAGAAAACCCCAAAAAUGAAGGGGACUAAAACAGGGGCAGAGAUGAUGACCCU-3'	Fig. 2b, ED4
Lbu_pre_cr_5'_mut8_AES498	5'-GGAUUUAGACCGCCCCAAAAAUGAAGGGGACUAAAACAGGGGCAGAGAUGAUGACCCU-3'	Fig. 2b, ED4
Lbu_pre_stem_mut1_AES502	5'-GGAUUUAGACCAGCCCAAAAAUGAAGGGCACUAAAACAGGGGCAGAGAUGAUGACCCU-3'	Fig. 2b, ED4
Lbu_pre_stem_mut2_AES501	5'-GGAUUUAGACCACCGCAAAAAUGAAGCGGACUAAAACAGGGGCAGAGAUGAUGACCCU-3'	Fig. 2b, ED4
Lbu_pre_stem_mut3_AES500	5'-GGAUUUAGACCACACCAAAAAUGAAGGUGACUAAAACAGGGGCAGAGAUGAUGACCCU-3'	Fig. 2b, ED4
Lbu_pre_stem_mut4_AES499	5'-GGAUUUAGACCACCACAAAAAUGAAGUGGACUAAAACAGGGGCAGAGAUGAUGACCCU-3'	Fig. 2b, ED4
Lbu_pre_stem_mut5_AES504	5'-GGAUUUAGACCACUCCAAAAAUGAAGGAGACUAAAACAGGGGCAGAGAUGAUGACCCU-3'	Fig. 2b, ED4
Lbu_pre_cr_3'_mut1_AES505	5'-GGAUUUAGACCACCCCAAAAAUGAAGGGGCAUAAAACAGGGGCAGAGAUGAUGACCCU-3'	Fig. 2b, ED4
Lbu_pre_cr_3'_mut2_AES506	5'-GGAUUUAGACCACCCCAAAAAUGAAGGGGACGCAAACAGGGGCAGAGAUGAUGACCCU-3'	Fig. 2b, ED4
Lbu_pre_cr_3'_mut3_AES507	5'-GGAUUUAGACCACCCCAAAAAUGAAGGGGACUAGCACAGGGGCAGAGAUGAUGACCCU-3'	Fig. 2b, ED4
Lbu_pre_cr_3'_mut4_AES508	5'-GGAUUUAGACCACCCCAAAAAUGAAGGGGACUAAAGUAGGGGCAGAGAUGAUGACCCU-3'	Fig. 2b, ED4
crLbu_A_GG_AES432	5'-GGCCACCCCAAAAAUGAAGGGGACUAAAACAGGGGCAGAGAUGAUGACCCU-3'	ED4-7
crLbu_B_AES451	5'-GGCCACCCCAAAAAUGAAGGGGACUAAAACACAAACAUGAUCUGGGUCAUC-3'	Fig. 3, ED 4
A.0_target_AES450	5'-GGCACACCCGCAGGGGGGAGCCAAAAGGGUCAUCAUCUCUGCCCCCACAGCAGAAGCCCC-3'	Fig. 3, ED4-7
B_target_AES452	5'-GGGAACCCCAAGGCCAACCGCGAGAAGAUGACCCAGAUCAUGUUUGAGACCUUCAACACCCC-3'	Fig. 3, ED4,6
crLbu_Lambda2_AES453	5'-GGCCACCCCAAAAAUGAAGGGGACUAAAACAGUGAUAAGUGGAAUGCCAUG-3'	Fig. 4b, ED 8
crLbu_Lambda3_MOC410	5'-GGCCACCCCAAAAAUGAAGGGGACUAAAACACUGGUGAACUUCCGAUAGUG-3'	Fig. 4b
crLbu_Lambda4_MOC411	5'-GGCCACCCCAAAAAUGAAGGGGACUAAAACACAGAUAUAGCCUGGUGGUUC-3'	Fig. 4b, ED 8
Lambda2_target_MOC28	5'-GGCUCAAUUUUGACAGCGGUCAUGGCAUUCCACUUAUCACUGGCAUCCUUCCACUC-3'	Fig. 4b, ED 8
Lambda3_target_MOC36	5'-GGAAAUCAUUCAACACCCGCACUAUCGGAAGUUCACCAGCCAGCCGCAGCACGUU-3'	Fig. 4b
Lambda4_target_MOC37	5'-GGCAAUAAAAAUGCGCCGCCUGAACCACCAGGCUAUAUCUGCCACUCAUUGUUGUGA-3'	Fig. 4b ED 8
crLbu_betaActin_1_AES451	5'-GGCCACCCCAAAAAUGAAGGGGACUAAAACACAAACAUGAUCUGGGUCAUC-3'	Fig. 4c
pre-crLbu_dimer_SCK324	5-'GGAUUUAGACCACCCCAAAAAUGAAGGGGACUAAAACAGGGGCAGAGAUGAUGACCCUAUUUAGACCACCCCAAAAAUGA AGGGGACUAAAACAGUGAUAAGUGGAAUGCCAUG-3'	Fig. 4d, ED3
crLbu_lambda2_SCK315	5'-GGAUUUAGACCACCCCAAAAAUGAAGGGGACUAAAACAGUGAUAAGUGGAAUGCCAUG-3'	ED3
Lbu_pre_cr_5'_4mer1_AES481	5'-GGAUUUAAUAAACCCCAAAAAUGAAGGGGACUAAAACAGGGGCAGAGAUGAUGACCCU-3'	ED3
Lbu_pre_cr_5'_4mer2_AES479	5'-GGAUUCGAUCCACCCCAAAAAUGAAGGGGACUAAAACAGGGGCAGAGAUGAUGACCCU-3'	ED3
Lbu_pre_cr_5'_4mer3_SCK343	5'-GGAUUUAGGAAGCCCCAAAAAUGAAGGGGACUAAAACAGGGGCAGAGAUGAUGACCCU-3'	ED3
Lbu_pre_cr_5'_4mer4_AES503	5'-GGAUUUAGACCAGGCCAAAAAUGAAGGCCACUAAAACAGGGGCAGAGAUGAUGACCCU-3'	ED3
crLbu_GuideWalk1_SCK302	5'-GGCCACCCCAAAAAUGAAGGGGACUAAAACAUUUUGGCUCCCCCCUGCAAAUGAG-3'	ED5
crLbu_GuideWalk2_SCK303	5'-GGCCACCCCAAAAAUGAAGGGGACUAAAACAACCCUUUUGGCUCCCCCCUGCAAA-3'	ED5
crLbu_GuideWalk3_SCK304	5'-GGCCACCCCAAAAAUGAAGGGGACUAAAACAGAUGACCCUUUUGGCUCCCCCCUG-3'	ED5
crLbu_GuideWalk4_SCK305	5'-GGCCACCCCAAAAAUGAAGGGGACUAAAACAAGAUGAUGACCCUUUUGGCUCCCC-3'	ED5
crLbu_GuideWalk5_SCK306	5'-GGCCACCCCAAAAAUGAAGGGGACUAAAACAGCAGAGAUGAUGACCCUUUUGGCU-3'	ED5
crLbu_GuideWalk6_SCK307	5'-GGCCACCCCAAAAAUGAAGGGGACUAAAACAGGGGGCAGAGAUGAUGACCCUUUU-3'	ED5
crLbu_GuideWalk7_SCK308	5'-GGCCACCCCAAAAAUGAAGGGGACUAAAACACAGAGGGGGCAGAGAUGAUGACCC-3'	ED5
crLbu_GuideWalk8_SCK309	5'-GGCCACCCCAAAAAUGAAGGGGACUAAAACAUCAGCAGAGGGGGCAGAGAUGAUG-3'	ED5
A.1_target_U_MOC279	5'-GGCUCAUUUGCAGGGGGGAGCCAAAAGGGUCAUCAUCUCUGCCCCCUCUGCUGAUGCCCC-3'	ED5
A.2_target_70nt_AES447	5'-GGCCUGACUGCUCUCAUUUGCAGUUGGGAGCCAAAAGGGUCAUCAUCUCUGCCCCCUCUGCUGAUGCCCC-3'	ED5
A.3_target_80nt_AES448	5'-GGACCUGUGAAUCCUGACUGCUCUCAUUUGCAGUUGGGAGCCAAAAGGGUCAUCAUCUCUGCCCCCUCUGCUGAUGCCCC-3'	ED5
A.4_5'_ts_shift_AES449	5'-GGCACACCCGCAGGGUUUAGCCAAAAGGGUCAUCAUCUCUGCCCCCUCUGCUGAUGCCCC-3'	ED5
crLbu_A_16nt_trunc_SCK282	5'-GGCCACCCCAAAAAUGAAGGGGACUAAAACACAGAGAUGAUGACCCU-3'	ED6
crLbu_A_24nt_ext_SCK283	5'-GGCCACCCCAAAAAUGAAGGGGACUAAAACAAGAGGGGGCAGAGAUGAUGACCCU-3'	ED6
crLbu_A_mature_GA_SCK340	5'-GACCACCCCAAAAAUGAAGGGGACUAAAACAGGGGCAGAGAUGAUGACCCU-3'	ED6
crLbu_A_mature_GGGA_SCK341	5'-GGGACCACCCCAAAAAUGAAGGGGACUAAAACAGGGGCAGAGAUGAUGACCCU-3'	ED6
crLbu_A_mature_CCA_AES461	5'-CCACCCCAAAAAUGAAGGGGACUAAAACAGGGGCAGAGAUGAUGACCCU-3'	ED6
T7 Forward (DNA)	5'-TAATACGACTCACTATAGG-3'	N/A

© 2016 Macmillan Publishers Limited, part of Springer Nature. All rights reserved.